Ionic liquid-modified microporous ZnCoNC-based electrocatalysts for polymer electrolyte fuel cells

Wang, Min; Zhang, Huixin; Thirunavukkarasu, Gnanavel; Salam, Ihtasham; Varcoe, John R.; Mardle, Peter; Li, Xiaoying; Mu, Shichun; Du, Shangfeng

DOI:
10.1021/acsenergylett.9b01407

Ionic liquid modified microporous ZnCoNC-based electrocatalysts for polymer electrolyte fuel cells

Min Wang[1,2], Huixin Zhang[2], Gnanavel Thirunavukkarasu[3], Ihtasham Salam[4], John R. Varcoe[4], Peter Mardle[2], Xiaoying Li[3], Shichun Mu[1], Shangfeng Du[2]*

[1]State Key Laboratory of Advanced Technology for Materials Synthesis and Processing, Wuhan University of Technology, Wuhan China

[2]School of Chemical Engineering, University of Birmingham, Birmingham UK

[3]School of Metallurgy and Materials, University of Birmingham, Birmingham UK

[4]Department of Chemistry, University of Surrey, Guildford UK

*Corresponding author: (Email: s.du@bham.ac.uk)

Abstract

Non-platinum group metal (non-PGM) oxygen reduction reaction (ORR) catalysts have been widely reported, but their application in proton exchange membrane fuel cells (PEMFCs) is challenging due to their poor performance in acidic environments. Here [BMIM][NTf_2] ionic liquid (IL) modification of microporous ZnCoNC catalysts (derived from ZIF-ZnCo) is investigated to study their behavior in PEMFCs and to elucidate the catalytic mechanisms in practical operation. The high O_2 solubility of ILs enhance the utilization of active sites with porous ZnCoNC and their hydrophobic nature facilitates the water transport during fuel cell operation. The half-cell measurement in aqueous $HClO_4$ shows that with the 20wt% IL modification, the electron transfer number increases from 2.58 to 3.88, approaching the desired 4-electron-transferred ORR. The power density obtained shows 140% improvement in single cell PEMFC tests. The catalyst also yields an interesting performance in alkaline anion-exchange membrane fuel cells (AEMFCs).

Table of Contents Graphic

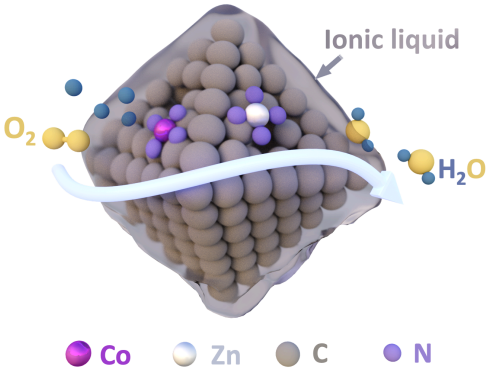

The hydrogen oxidation reaction (HOR) and oxygen reduction reaction (ORR) occur in the anode and cathode, respectively, of polymer electrolyte fuel cells (PEFCs), such as proton exchange membrane fuel cells (PEMFCs) or alkaline anion-exchange membrane fuel cell (AEMFC). Both reactions typically involve Pt-based catalysts, which are expensive and unsustainable.[1] The ORR exhibits poor kinetics, and therefore PEMFCs generally require large amounts of Pt at the cathode.[2,3] This is a major driver for researchers to develop cheaper and more sustainable alternatives.

A widely reported class of non-platinum group metal (non-PGM) ORR catalysts involve Fe-, Co- and N-doped carbon materials (Fe,Co-N/C).[4,5] Among them, Fe,Co-N/C-based ORR catalysts derived from zeolitic imidazolate frameworks (ZIF) have received considerable attention in recent years.[6] The products of carbonizing ZIFs usually inherit the parent's structure features and can result in heteroatom-doped, or metal nanoparticle-containing, microporous carbons with excellent ORR activities.[6–8] For instance, single Co atom-based N-doped carbons can be made by pyrolyzing ZIF-ZnCo in N_2,[7,9] while single Fe atom variants can be prepared by heating ZIF-8 and $Fe(acac)_4$ in inert gas;[10] both of these types have been reported to show better ORR activities and stabilities than Pt/C catalysts in alkaline electrolytes. However, despite great progress with Fe,Co-N/C-based catalysts, they still show inferior performances compared to Pt/C catalysts in acidic electrolytes.[11] As a consequence, with the application of Fe,Co-N/C catalysts in PEMFCs, a much thicker cathode catalyst layer (with a higher catalyst loading) is usually required (*cf.* Pt/C cathodes), which severely hinders mass transport within the catalyst layers and results in very low catalyst utilization and poor power performance.[4] Further improvements in the ORR activities of non-PGM catalysts in acidic conditions is desired.

It has been found that increasing the specific surface area (SSA)[12] and the concentration of ORR active species (*e.g.* Fe/Co-N_4,[13,14] nitrogen sites,[15] defects,[16] metal compounds nanoparticles[17]) generally leads to improved ORR performance. Previous work has also shown that catalytic sites are inactive at a depth of several tens of nanometers into the catalyst due to O_2 transport limitations.[18] Hence, continually increasing SSA will not lead to a consistent enhancement in ORR activity. Catalysts that perform well in alkaline electrolyte often exhibit significantly poorer ORR activity in acidic environments, due to the low activities of doped nitrogen sites at low pH.[16] Meanwhile, further increasing the concentration of Fe/Co-N_4 active sites becomes difficult due to the tendency of the doped metal to aggregate, directly leading to performance decreases.[4] Therefore, an alternative approach for increasing the ORR performance of such catalysts in PEMFCs is urgently needed.

Adjusting the nature of the interface where ORR occurs using ionic liquids (ILs) is a new, promising method being investigated. In 2010, Erlebacher *et al.* modified a nanoporous PtNi catalyst with [MTBD][beti], a hydrophobic and protonic IL with high O_2 solubility.[18] This modification showed an effective improvement in ORR performance. After that, a range of ILs have been employed to modify PtNi, Pt/Graphene and commercial Pt/C catalysts, leading to enhanced mass activities and stabilities.[19–22] In 2017, Titirici *et al.* used ILs to modify, for the first time, non-PGM carbon-based ORR electrocatalysts where the activities showed notable improvement in both basic and acidic electrolytes.[23] Subsequently, it was reported by Kramm *et al.* that ILs improved the ORR activity of Fe-N/C catalysts in alkaline electrolyte.[24] However, IL modification of transition metal-based ORR catalysts are still rarely reported, especially for Co-N/C based materials. The practical

behavior and operational mechanisms of such IL-modified non-PGM catalysts in fuel cells remain unknown, as they have not been rigorously tested in either PEMFCs or AEMFCs.

In this study, we synthesized porous ZIF-ZnCo materials and carbonized them to prepare a microporous carbon matrix doped by Zn, Co and N atoms (denoted as ZnCoNC from hereon). [BMIM][NTf_2] (1-butyl-3-methylimidazolium bis(trifluoromethylsulfonyl)imide), a hydrophobic aprotic IL, was used to further modify the ZnCoNC catalysts using a facile adsorption method that utilized the capillary action of ILs in the porous media. The effect of the IL loading level was studied, and an optimized catalyst was evaluated in both acidic and alkaline environments. Better activities were observed in half-cell electrochemical measurements (*cf.* the IL-free benchmarks), and higher *in situ* power densities were also obtained in both PEMFCs and AEMFCs.

As illustrated in **Figure 1a**, the IL-modified ZnCoNC catalysts are prepared using three steps: (1) the precursor (ZIF-ZnCo) is formed *via* the assembly of Zn^{2+}, Co^{2+} ions with 2-methylimidazole (DMI); (2) ZIF-ZnCo is transformed into Zn,Co/N-atoms-doped microporous carbon (ZnCoNC) *via* carbonization at 900°C under N_2; and (3) the IL-modified ZnCoNC catalysts are obtained on immersion of ZnCoNC in IL-containing solutions (followed by vacuum drying in a desiccator until all solvent is removed). The IL-modified ZnCoNC catalysts obtained are designated ZnCoNC-ILx (x presents the weight percentage of IL to ZnCoNC).

The SEM and TEM images of ZnCoNC catalyst are shown in **Figure S1a** and **Figure 1b**, respectively. The ZnCoNC catalyst has polyhedron-shaped particles with sizes in the range 300 – 500 nm and with distinct facets and edges (**Figure 1b**). ZnCoNC-IL20 (ZnCoNC containing 20 wt% IL) retains the same particle shape (**Figure S1b** and **Figure**

S1c), implying the IL deposited into the microporous ZnCoNC matrix does not alter morphology to any great extent. The high-resolution TEM (HRTEM) images of pre-IL-treated ZnCoNC (**Figure 1c**) and ZnCoNC-IL20 (**Figure 1d)** highlight the distinct edges and exhibit uniform greyscale contrasts indicating no major metal aggregation occurred. The elemental mapping of ZnCoNC-IL20 is displayed in **Figure 1e**. N-, Zn- and Co-mapping reveal that N, Zn and Co atoms are uniformly distributed over the entire carbon matrix, while F- and S-mapping indicate the uniform adsorption of IL into ZnCoNC carbon matrix.

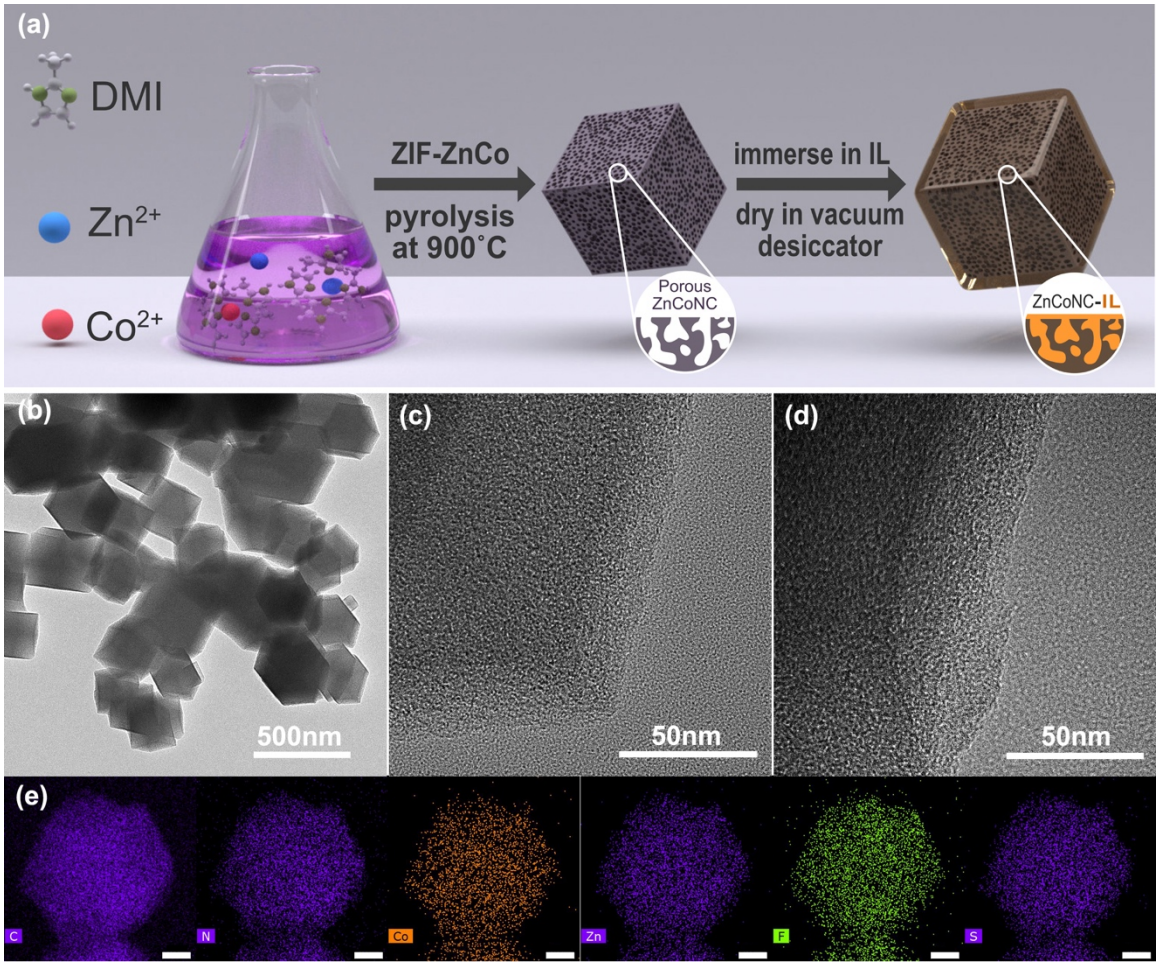

Figure 1. (a) Schematic outline of the preparation of the IL-modified ZnCoNC catalysts. (b) TEM and (c) HRTEM images of ZnCoNC catalyst. (d) HRTEM image of the ZnCoNC-IL20 catalyst with (e) the corresponding elemental maps (scale bar, 100 nm).

The X-ray diffraction (XRD) patterns of ZIF-ZnCo and different amounts of IL modified ZnCoNC catalysts are shown in **Figure 2a**. The diffraction peaks of the precursor ZIF-ZnCo match the XRD patterns of ZIFs prepared in other works.[7,9] After thermal treatment, only a broad peak at $2\theta = 25°$ is observed for ZnCoNC-IL0, suggesting the ZIF-ZnCo are transformed into heteroatom-doped amorphous carbon. This result is consistent with above TEM analysis results and previous work.[25] The different levels of IL modification give ZnCoNC catalysts (ZnCoNC-IL0.2, ZnCoNC-IL2, ZnCoNC-IL20, ZnCoNC-IL200) similar XRD patterns to that of ZnCoNC-IL0, indicating the IL retains its amorphous structure after being absorbed into the ZnCoNC catalysts.

The specific surface area (SSA) and pore width distribution (PWD) of ZnCoNC-IL0 and ZnCoNC-IL20 were evaluated using N_2 sorption at room temperature (**Figure 2b** and inset). Both ZnCoNC-IL0 and ZnCoNC-IL20 have sharp peaks at 0.66 nm and 0.82 nm, respectively, suggesting a microporous structure for both. The PWD of ZnCoNC-IL20 shows a positive shift (*cf.* ZnCoNC-IL0). In addition, the SSA of ZnCoNC-IL0 is 649 m^2 g^{-1}, significantly higher than that of ZnCoNC-IL20 (43 m^2 g^{-1}). Meanwhile, the total pore volume (PV, 0.07 cm^3 g^{-1}) of ZnCoNC-IL20 is reduced by 97% compared to the control ZnCoNC-IL0 (PV = 2.79 cm^3 g^{-1}). The PWD shift, drop of SSA and PVs for ZnCoNC-IL20 indicates the IL filling the micropores of the ZnCoNC carbon matrix.

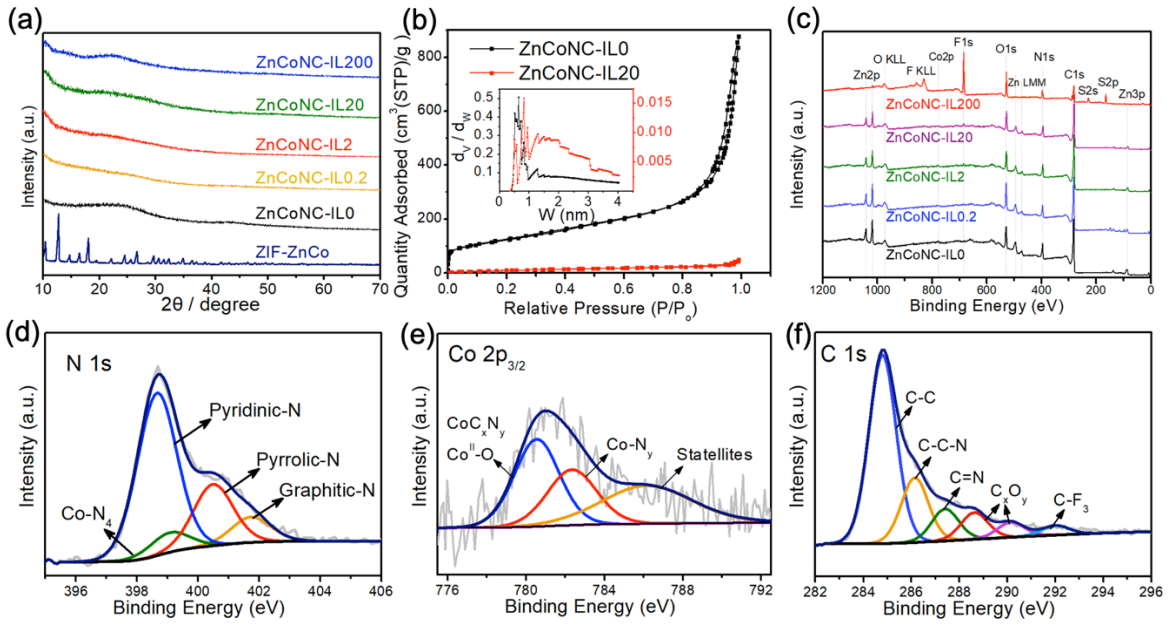

Figure 2. (a) Powder XRD patterns of ZIF-ZnCo and the IL-modified ZnCoNC catalysts (with different levels of IL incorporation). (b) N_2 adsorption/desorption isotherms of ZnCoNC-IL0 and ZnCoNC-IL20 (the inset gives the pore width distributions). (c) XPS spectra of ZnCoNC-IL0 and the IL modified ZnCoNC catalysts with band deconvolution for ZnCoNC-IL20 given in the following specific high resolution XPS regions: (d) N 1s, (e) Co $2p_{3/2}$, and (f) C 1s.

To better understand the composition of the obtained catalysts, X-ray photoelectron spectroscopy (XPS) analysis was conducted on the ZnCoNC catalyst with and without IL modification (**Figure 2c**) with the percentage contents of each element listed in **Table S1**. ZnCoNC-IL0 contains five elements (4.66% Co, 10.52% N, 45.11% C, 14.68% O and 25.03% Zn) on the particle surfaces, while two new elements (F, S) appear after the IL modification (ZnCoNC-IL0.2 to ZnCoNC-IL200) with percentages that raise with an increase in the IL content. When 20 wt% of IL is loaded onto the ZnCoNC catalyst, the percentages of F and S increase to 2.61% and 0.89%, respectively, whereas the percentage of Co and Zn drop to 2.03% and 17.9%, respectively, which is consistent with a thin layer

of IL covering surface of the ZnCoNC particles. When 200 wt% of IL is added, the Co signal is barely detectible and the Zn content dramatically reduces to 1.94%, suggesting a thick layer of IL formed on the ZnCoNC particles.

For ZnCoNC-IL20, the high-resolution N 1s spectrum exhibited in **Figure 2d** can be fitted with four peaks, which correspond to pyridinic-N (398.6 eV), Co-N_4 (399.15 eV), pyrrolic-N (400.5 eV) and graphitic-N (401.7 eV).[9,26] The Co $2p_{3/2}$ XPS spectrum (**Figure 2e**) can be fitted with three peaks located at 780.56 eV, 782.37 eV, and 786.13 eV, corresponding to Co^{II}-O (or CoC_xN_y), Co-N_y, and the satellite peak, respectively.[9,25] The formation of Co-N_4 (N 1s spectrum) and Co-N_y (in Co $2p_{3/2}$ spectrum) indicates the existence of atomically dispersed Co atoms. In the high-resolution C 1s region (**Figure 2f**), the three main peaks observed at 284.7 eV, 286.2 eV, and 287.3 eV correspond to C-C, C-C-N and C=N, respectively. The minor peaks at 288.6 eV and 290.2 eV relate to C_xO_y, while the weakest peak at 292.0 eV is characteristic of C-F_3 from the IL.[27,28] The high resolution Zn $2p_{2/3}$ spectrum (**Figure S2**) shows a peak at 1022.8 eV assigned to Zn-N_4[29] which is also the active site for ORR.[30]

The ORR activities of the as-prepared catalysts in acid environment (aqueous 0.1 M $HClO_4$) were first studied using half-cell electrochemical measurements. The liner-sweep voltammetry (LSV) curves for ZnCoNC-IL0 and the catalysts containing increasing amounts of IL are shown in **Figure 3a**. The ZnCoNC-IL0 catalyst exhibits an onset potential (Eo) of 0.55 V *vs.* Ag/AgCl and a limited current density (J_{limit}) of 5.32 mA cm^{-2}, which are lower than the commercial Pt/C catalyst (**Figure S3a**) but comparable to other Co-based catalysts (**Table S2**)[9,25] The J_{limit} obtained with the catalysts initially increase with the IL loading (up to 20 wt%) before declining again as the IL contents continue to

increase. The J_{limit} value of ZnCoNC-IL20 is *ca.* 160% of that obtained with the control ZnCoNC-IL0 catalyst. This improvement is in accord with the results reported for other IL-modified non-PGM ORR catalysts.[23,24] The EIS Nyquist plots (**Figure S3b**) for all catalysts show that the Ohmic resistances decrease with the increasing IL. The average electron transfer number (n_e) for each catalyst was calculated based on the slope of the K-L plots derived from the recorded LSV curves (O_2 saturated electrolyte) measured at different rotation rates (**Figure S4a-e**) and plotted as a function of the IL content in **Figure 3b**. This data exhibits the same trend to that of J_{limit}: highest values obtained with ZnCoNC-IL20 with n_e = 3.88 (150% the value obtained with ZnCoNC-IL0), which is very close to the ideal (non-H_2O_2-generating) 4e^--transferred ORR. The improvement can be ascribed to the high O_2 solubility in the IL filled micropores, resulting in dual-active-site adsorption of O-O (rather than end-on adsorption of O-O on a single active site) and a higher concentration of reactants at the active sites (Co-N_4, Zn-N_4), thus improving catalyst utilization and facilitating 4-electron ORR.[18,22,23] This is further confirmed by a reduced Tafel slope from 78 mV/dec of ZnCoNC-IL0 to 62 mV/dec of ZnCoNC-IL20 (**Figure S4f**). The decline in J_{limit} with higher IL contents relates to the high surface tension nature of the IL: a larger amount of IL will tend to form isolated islands of thick IL films on the surface of the ZnCoNC carbon matrix rather than penetrating into the micropores, reducing the internal O_2 concentration of ZnCoNC carbon matrix (leading to a lower J_{limit}).[18,22]

Figure 3c compares the electrochemical stabilities of ZnCoNC-IL0 and ZnCoNC-IL20 in 0.1 M O_2-saturated $HClO_4$(aq), which were evaluated using an accelerated degradation test (ADT, 5000 potential sweep cycles). After the ADT, both catalysts show reduced diffusion-controlled currents and kinetic currents occurring with lower onset potentials.

Despite ZnCoNC-IL20 showing a larger drop in J_{limit} than ZnCoNC-IL0 after cycling (possibly due to loss of some weakly adsorbed ILs along with catalyst corrosion processes), it still shows a better ORR profile than ZnCoNC-IL0, with J_{limit} being ca. 1.53 times suggesting most IL content is retained in the micropores. To further elucidate the degradation mechanisms, HRTEM analysis was conducted on both post-ADT samples (**Figure 3d-g**). Both catalysts retained the polyhedron-shaped carbon matrix, but with rougher edges due to ADT-derived corrosion processes. Compared to the much coarser edges of ZnCoNC-IL0 (**Figure 3d** and **3e**), ZnCoNC-IL20 (**Figure 3f** and **3g**) keeps the distinct edges and faces better to a considerable degree after the ADT, indicating a positive protecting effect from the IL coating which partially blocks the direct contact of catalyst surface with acid causing corrosion. The elemental maps and element contents of ZnCoNC and ZnCoNC-IL20 after the ADT were obtained by Energy-dispersive X-ray spectroscopy (EDS) (**Figure S5** and **Table S3**). After the ADT, both catalysts show a significant decrease of the Co and Zn contents, corresponding the loss of active sites. However, ZnCoNC-IL20 remains much more Co and Zn than ZnCoNC-IL0. **Table S3** indicates a Co and Zn content of 0.07% and 0.93% from initial 0.12% and 5.16%, respectively, for ZnCoNC-IL20 after the ADT, but these values are only 0.04% and 0.59%, respectively, for ZnCoNC-IL0. This implies the positive role of the IL in protecting the active sites from corrosion, as well as the poor stability of Zn and Co in acid electrolyte in the ADT.

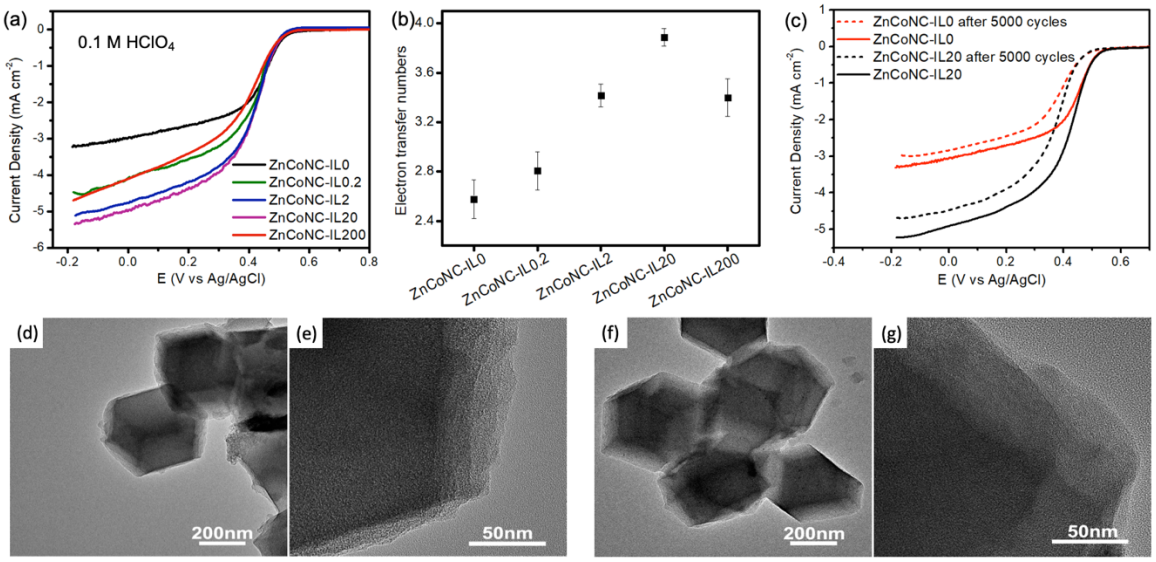

Figure 3. (a) ORR LSV curves of the obtained catalysts tested in O_2 saturated 0.1 M $HClO_4$(aq) at a rotation rate of 1600 rpm (Scan rate = 20 mV s^{-1}), and (b) corresponding average electron transfer numbers (n_e). (c) LSV curves of ZnCoNC-IL0 and ZnCoNC-IL20 before and after 5000 potential sweep cycles (between 0.3 – 0.7 V at 200 mV s^{-1}) in O_2 saturated 0.1 M $HClO_4$(aq). Comparison of HRTEM images of (d,e) ZnCoNC-IL0 and (f,g) ZnCoNC-IL20 after 5000 potential sweep cycles (between 0.3 – 0.7 V at 200 mV s^{-1}) in O_2 saturated 0.1 M $HClO_4$(aq).

To further evaluate the impact of ILs on the ORR performance of the ZnCoNC catalysts in PEMFC operation, membrane electrode assemblies (MEAs) containing ZnCoNC-IL0 and ZnCoNC-IL20 cathodes were tested in H_2/air single-cell PEMFC (active area of 16 cm^2). The polarization and power density curves are shown in **Figure 4a**. ZnCoNC-IL20 shows the higher power performance (peak power density increased by ca. 140% compared with ZnCoNC-IL0) although the absolute value is still low. The dramatic improvement of ORR activity in the PEMFC can be contributed by the enhanced electron transfer number as discussed above and the high O_2 affinity of the fluorinated side chains of $[NTf_2]^-$ anions

which increases the O_2 concentration in the ZnCoNC carbon matrix,[31] as well as the hydrophobic character of the IL which help to expel the generated water in catalyst layer freeing up active sites in operation and therefore improve the power performance.[23] Electrochemical impedance spectroscopy (EIS) spectral data (**Figure 4b**) shows that the presence of IL leads to a decrease of charge-transfer resistance (with a concomitant small decrease in Ohmic resistance). Based on the above results, we can conclude that optimal IL modification of the ZnCoNC catalysts can efficiently improve the ORR activity. However, the optimal amount will depend on the surface tension of ILs, the size distribution of pores as well as the interaction between the catalyst and IL, which all need to be determined experimentally in future research on different catalyst-IL combinations.

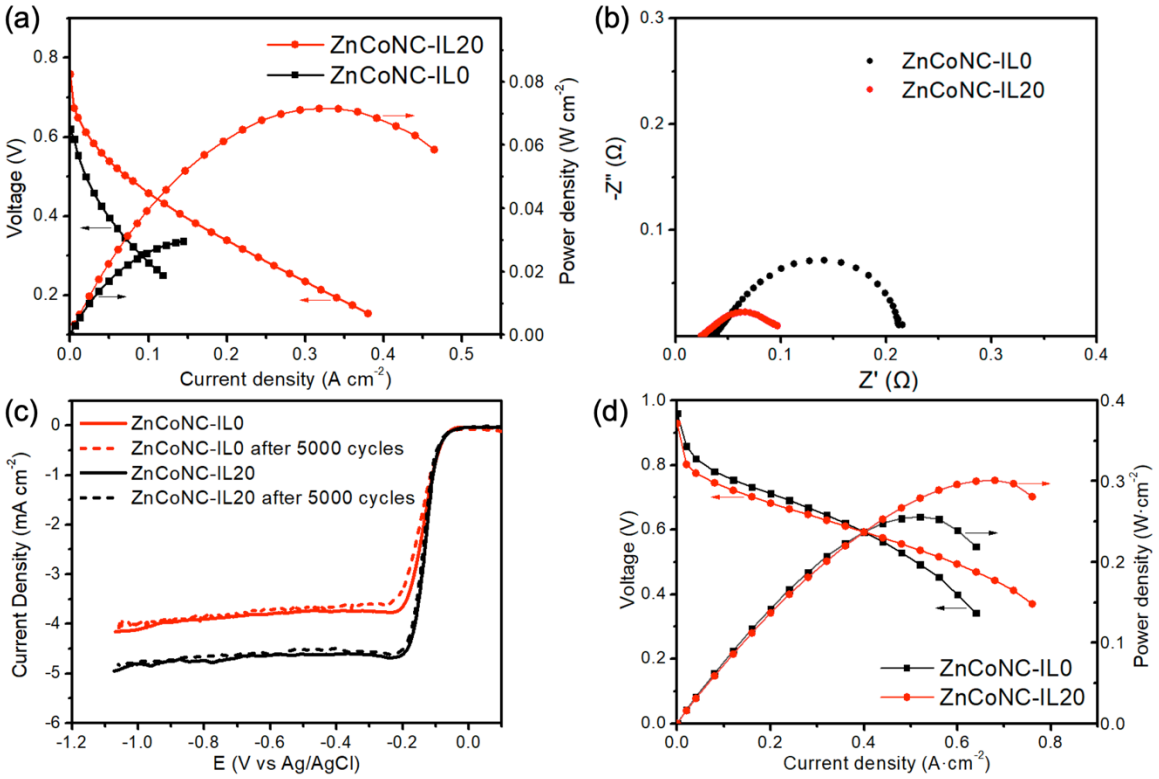

Figure 4. (a) H_2/air single-cell PEMFC polarization plots (80°C cell temperature, cathode = 2 mg_{ZnCoNC} cm^{-2} and anode = 0.4 mg_{Pt} cm^{-2}) with H_2/air (fully hydrated) supplied with

stoichiometries= 1.3/2.4. (b) EIS spectra measured at a cell voltage of 0.5. (c) LSV curves of ZnCoNC-IL0 and ZnCoNC-IL20 before and after ADT (5000 cycles of CV scans between -0.4 – 0.1 V at 200 mV s^{-1}) tested in O_2 saturated 0.1 M KOH(aq) (rotation rate: 1600 rpm, scan rate: 20 mV s^{-1}). (d) H_2/O_2 AEMFC polarization plots (70°C, cathode = 0.78 mg_{ZnCoNC} cm^{-2} and anode = 0.6 mg_{PtRu} cm^{-2}).

For scientific completeness, the ORR activities of ZnCoNC-IL20 and ZnCoNC-IL0 were also evaluated under alkaline conditions using both half-cell electrochemical measurements with aqueous 0.1 M KOH(aq) electrolyte and in anion-exchange membrane fuel cells (AEMFCs). The LSV data for both down-selected catalysts before and after ADT (5000 potential sweeping cycles, -0.4 – 0.1 V sweep range, 200 mV s^{-1}) were tested in O_2 saturated 0.1 M KOH(aq) (**Figure 4c**). The as-synthesized ZnCoNC-IL0 shows an E_o of -0.015 V (*vs.* Ag/AgCl) and half wave potential ($E_{1/2}$) of -0.14 V (*vs.* Ag/AgCl) which are comparable with the commercial Pt/C catalyst (**Figure S3a**) and recently reported single Co atom doped ORR catalysts (**Table S2**).[7,32] Before the ADT, ZnCoNC-IL20 yielded a higher (~22.6%) J_{limit} than ZnCoNC-IL0. It also has a lower Ohmic resistances (**Figure S6a**) and a higher n_e (**Figure S6b** and **S6c**) than ZnCoNC-IL0. After the stability test, in contrast to the tests in acid, both catalysts exhibited excellent stability (**Figure 4c**) with a less significant decrease in limited current density (and half wave potential).

The polarization curves for ZnCoNC-IL0 and ZnCoNC-IL20 in single-cell AEMFCs (**Figure 4d**) show the same trend as the half-cell LSV measurements (**Figure 4c**). ZnCoNC-IL20 shows a higher power density in the low voltage, mass-transport region (0.3 – 0.6 V), but a slightly larger overpotential compared to ZnCoNC-IL0 in the high voltage, kinetic region (> 0.6 V). The better performance in the mass-transport region can be

ascribed to the improved water repelling properties due to the hydrophobic feature of the IL and the high O_2 affinity of the fluorinated side chains of $[NTf_2]^-$ anions.[23,31] In the kinetic region, the lower power performance can be potentially explained through the attacking of the IL cations by OH^- and superoxide ion (*e.g.* $O_2^{\bullet-}$) in fuel cell operation. Specifically, the OH^- and $O_2^{\bullet-}$ ($O_{2,ads} + e^- \rightarrow O_{2,ads}^{\bullet-}$, the first step of ORR in both acid and alkaline electrolyte) can attack the proton at the C2-position of the imidazolium cation $[BMIM]^+$ in the IL molecule, and then one of the C−N bonds is broken resulting in an open imidazole ring.[33,34] As water molecules in fuel cell operation are H-bonded to the IL cations and anions,[35–37] the degradation of IL cations makes water transfer difficult and therefore slowing down the following ORR step ($O_{2,ads}^{\bullet-} + H_2O \rightarrow HO_{2,ads}^{\bullet-} + OH^-$).[38] The consuming of $O_2^{\bullet-}$ also defers the proceeding of ORR. For this attacking and the super hydrophobicity of ILs, the increase of temperature will make them worse and this is confirmed by fuel cell test results at a higher operation temperature. When the AEMFC operation temperature increases from 70˚C to 80˚C (**Figure S7**), ZnCoNC-IL0 shows an improved power performance, but declining for ZnCoNC-IL20.

Comparing the data in acidic and alkaline environment, in both half-cell measurements and fuel cell tests, it can be found that the performance enhancement on IL-modification is more effective in acid than that in alkaline, although power outputs are still low in PEMFC tests for this non-PGM ZnCoNC catalyst. The positive effect of using the $[BMIM][NTf_2]$ IL to modify the catalysts has previously been confirmed in both acid and alkaline aqueous electrolytes by half-cell measurement.[22,23] However, in practical fuel cells, the mechanisms operating can be different to those observed in aqueous liquid electrolytes. Although $[BMIM][NTf_2]$ is aprotic, it is reported that the trace amount of water in such hydrophobic

ILs can form a percolating network,[39–41] which can aid H^+ transportation (through direct hydronium diffusion or proton hopping between hydronium and water molecules).[20,22] In this case, adding IL not only promotes electron transfer but also increases H^+ mobility,[41] leading to improved power performances. However, in AEMFCs, only conductivity and O_2 concentration is promoted.[22] Hence, we only observe an improved power performance in the low potential range. Therefore, to develop a higher performance fuel cells that use IL-modified catalysts, the selection of ILs will play a very important role.

In conclusion, a promising strategy is demonstrated that improves the operating performance of fuel cells containing non-PGM ORR catalysts by modification with ionic liquids. The stable adsorption of the IL in the micropores of a Zn, Co and N atoms doped carbon catalysts (ZnCoNC) improved the current density, electronic conductivity, and electron transfer number in acid electrolytes as well as the *in situ* performance in operating PEMFCs. The optimal IL content was found to be 20 wt%. A further evaluation in AEMFC was also conducted, which showed more complex trends on IL modification. Future research will require a careful selection of IL for use in different applications (with different pH environments).

ASSOCIATED CONTENT

The Supporting Information is available free of charge on the ACS Publications website at …Experimental section, SEM images, TEM images, XPS spectrum, LSV curves, Tafel plots, Nyquist plots, XPS analysis results, EDS results, summary of ORR activity.

AUTHOR INFORMATION

Corresponding Author *Email: s.du@bham.ac.uk

Notes

The authors declare no competing financial interest.

ACKNOWLEDGMENT

M Wang would like to thank the China Scholarship Council (CSC) for supporting her one-year study at the University of Birmingham. HX Zhang is funded by EU H2020 Marie Skłodowska-Curie Fellowship (739940). The fuel cell testing was conducted by materials produced using funding awarded by the UK's Engineering and Physical Sciences Research Council (grant EP/M014371/1 and EP/L015749/1). Thanks are also due to Mr. Yushi Yang from the University of Bristol for his constructive comments and paper revisions for the work.

REFERENCES

(1) Li, W.; Hu, Z.; Zhang, Z.; Wei, P.; Zhang, J.; Pu, Z.; Zhu, J. Nano-Single Crystal Coalesced PtCu Nanospheres as Robust Bifunctional Catalyst for Hydrogen Evolution and Oxygen Reduction Reactions. *J. Catal.* **2019**, *375*, 164–170.

(2) Guo, C.; Zheng, Y.; Ran, J.; Xie, F.; Jaroniec, M.; Qiao, S. Z. Engineering High-Energy Interfacial Structures for High-Performance Oxygen-Involving Electrocatalysis. *Angew. Chemie - Int. Ed.* **2017**, *56* (29), 8539–8543.

(3) Majlan, E. H.; Rohendi, D.; Daud, W. R. W.; Husaini, T.; Haque, M. A. Electrode for Proton Exchange Membrane Fuel Cells: A Review. *Renew. Sustain. Energy Rev.* **2018**, *89*, 117–134.

(4) Banham, D.; Choi, J.-Y.; Kishimoto, T.; Ye, S. Integrating PGM-Free Catalysts into Catalyst Layers and Proton Exchange Membrane Fuel Cell Devices. *Adv. Mater.* **2019**, 1804846.

(5) Shao, M.; Chang, Q.; Dodelet, J.-P.; Chenitz, R. Recent Advances in Electrocatalysts for Oxygen Reduction Reaction. *Chem. Rev.* **2016**, *116* (6), 3594–3657.

(6) Yang, L.; Zeng, X.; Wang, W.; Cao, D. Recent Progress in MOF-Derived, Heteroatom-Doped Porous Carbons as Highly Efficient Electrocatalysts for Oxygen Reduction Reaction in Fuel Cells. *Adv. Funct. Mater.* **2018**, *28* (7), 1–21.

(7) Yin, P.; Yao, T.; Wu, Y.; Zheng, L.; Lin, Y.; Liu, W.; Ju, H.; Zhu, J.; Hong, X.; Deng, Z. Single Cobalt Atoms with Precise N-coordination as Superior Oxygen Reduction Reaction Catalysts. *Angew. Chem., Int. Ed.* **2016**, *55* (36), 10800–10805.

(8) Park, K. S.; Ni, Z.; Cote, A. P.; Choi, J. Y.; Huang, R.; Uribe-Romo, F. J.; Chae, H. K.; O'Keeffe, M.; Yaghi, O. M. Exceptional Chemical and Thermal Stability of Zeolitic Imidazolate. *Proc. Natl. Acad. Sci.* **2006**, *103* (27), 10186–10191.

(9) Wang, X. X.; Cullen, D. A.; Pan, Y. T.; Hwang, S.; Wang, M.; Feng, Z.; Wang, J.; Engelhard, M. H.; Zhang, H.; He, Y.; et al. Nitrogen-Coordinated Single Cobalt Atom Catalysts for Oxygen Reduction in Proton Exchange Membrane Fuel Cells. *Adv. Mater.* **2018**, *30* (11), 1–11.

(10) Chen, Y.; Ji, S.; Wang, Y.; Dong, J.; Chen, W.; Li, Z.; Shen, R.; Zheng, L.; Zhuang, Z.; Wang, D.; et al. Isolated Single Iron Atoms Anchored on N-Doped

Porous Carbon as an Efficient Electrocatalyst for the Oxygen Reduction Reaction. *Angew. Chem., Int. Ed.* **2017**, *56* (24), 7003–7003.

(11) Wu, G.; Zelenay, P. Nanostructured Nonprecious Metal Catalysts for Oxygen Reduction Reaction. *Acc. Chem. Res.* **2013**, *46* (8), 1878–1889.

(12) Yang, W.; Fellinger, T. P.; Antonietti, M. Efficient Metal-Free Oxygen Reduction in Alkaline Medium on High-Surface-Area Mesoporous Nitrogen-Doped Carbons Made from Ionic Liquids and Nucleobases. *J. Am. Chem. Soc.* **2011**, *133* (2), 206–

(13) Zagal, J. H. J. H.; Koper, M. T. M. M. Reactivity Descriptors for the Activity of Molecular MN_4 Catalysts for the Oxygen Reduction Reaction. *Angew. Chem., Int. Ed.* **2016**, *55* (47), 14510–14521.

(14) Fei, H.; Dong, J.; Feng, Y.; Allen, C. S.; Wan, C.; Volosskiy, B.; Li, M.; Zhao, Z.; Wang, Y.; Sun, H.; et al. General Synthesis and Definitive Structural Identification of MN_4C_4 Single-Atom Catalysts with Tunable Electrocatalytic Activities. *Nat. Catal.* **2018**, *1* (1), 63–72.

(15) Guo, D.; Shibuya, R.; Akiba, C.; Saji, S.; Kondo, T.; Nakamura, J. Active Sites of Nitrogen-Doped Carbon Materials for Oxygen Reduction Reaction Clarified Using Model Catalysts. *Science* **2016**, *351* (6271), 361–365.

(16) Tang, C.; Wang, H. F.; Chen, X.; Li, B. Q.; Hou, T. Z.; Zhang, B.; Zhang, Q.; Titirici, M. M.; Wei, F. Topological Defects in Metal-Free Nanocarbon for Oxygen Electrocatalysis. *Adv. Mater.* **2016**, *28* (32), 6845–6851.

(17) Wang, M.; Zhang, C.; Meng, T.; Pu, Z.; Jin, H.; He, D.; Zhang, J.; Mu, S. Iron Oxide and Phosphide Encapsulated within N,P-Doped Microporous Carbon Nanofibers as Advanced Tri-Functional Electrocatalyst toward Oxygen

Reduction/Evolution and Hydrogen Evolution Reactions and Zinc-Air Batteries. *J. Power Sources* **2019**, *413*, 367–375.

(18) Snyder, J.; Fujita, T.; Chen, M. W.; Erlebacher, J. Oxygen Reduction in Nanoporous Metal-Ionic Liquid Composite Electrocatalysts. *Nat. Mater.* **2010**, *9* (11), 904–907.

(19) Tan, Y.; Xu, C.; Chen, G.; Zheng, N.; Xie, Q. A Graphene-Platinum Nanoparticles-Ionic Liquid Composite Catalyst for Methanol-Tolerant Oxygen Reduction Reaction. *Energy Environ. Sci.* **2012**, *5* (5), 6923–6927.

(20) Snyder, J.; Livi, K.; Erlebacher, J. Oxygen Reduction Reaction Performance of [MTBD][Beti]-Encapsulated Nanoporous NiPt Alloy Nanoparticles. *Adv. Funct. Mater.* **2013**, *23* (44), 5494–5501.

(21) Zhang, G.-R.; Munoz, M.; Etzold, B. J. M. Boosting Performance of Low Temperature Fuel Cell Catalysts by Subtle Ionic Liquid Modification. *ACS Appl. Mater. Interfaces* **2015**, *7* (6), 3562–3570.

(22) Zhang, G. R.; Munoz, M.; Etzold, B. J. M. Accelerating Oxygen-Reduction Catalysts through Preventing Poisoning with Non-Reactive Species by Using Hydrophobic Ionic Liquids. *Angew. Chem., Int. Ed.* **2016**, *55* (6), 2257–2261.

(23) Qiao, M.; Tang, C.; Tanase, L. C.; Teodorescu, C. M.; Chen, C.; Zhang, Q.; Titirici, M. M. Oxygenophilic Ionic Liquids Promote the Oxygen Reduction Reaction in Pt-Free Carbon Electrocatalysts. *Mater. Horizons* **2017**, *4* (5), 895–899.

(24) Martinaiou, I.; Wolker, T.; Shahraei, A.; Zhang, G. R.; Janßen, A.; Wagner, S.; Weidler, N.; Stark, R. W.; Etzold, B. J. M.; Kramm, U. I. Improved

Electrochemical Performance of Fe-N-C Catalysts through Ionic Liquid Modification in Alkaline Media. *J. Power Sources* **2018**, *375*, 222–232.

(25) Li, Z. H.; Shao, M. F.; Zhou, L.; Zhang, R. K.; Zhang, C.; Wei, M.; Evans, D. G.; Duan, X. Directed Growth of Metal-Organic Frameworks and Their Derived Carbon-Based Network for Efficient Electrocatalytic Oxygen Reduction. *Adv. Mater.* **2016**, *28* (12), 2337–2344.

(26) Pels, J. R.; Kapteijn, F.; Moulijn, J. A.; Zhu, Q.; Thomas, K. M. Evolution of Nitrogen Functionalities in Carbonaceous Materials during Pyrolysis. *Carbon* **1995**, *33* (11), 1641–1653.

(27) Beattie, D. A.; Arcifa, A.; Delcheva, I.; Le Cerf, B. A.; MacWilliams, S. V.; Rossi, A.; Krasowska, M. Adsorption of Ionic Liquids onto Silver Studied by XPS. *Colloids Surfaces A* **2018**, *544*, 78–85.

(28) Reshetenko, T.; Serov, A.; Artyushkova, K.; Matanovic, I.; Stariha, S.; Atanassov, P. Tolerance of Non-Platinum Group Metals Cathodes Proton Exchange Membrane Fuel Cells to Air Contaminants. *J. Power Sources* **2016**, *324*, 556–571.

(29) Killian, M. S.; Gnichwitz, J. F.; Hirsch, A.; Schmuki, P.; Kunze, J. ToF-SIMS and XPS Studies of the Adsorption Characteristics of a Zn-Porphyrin on TiO_2. *Langmuir* **2010**, *26* (5), 3531–3538.

(30) Song, P.; Luo, M.; Liu, X.; Xing, W.; Xu, W.; Jiang, Z.; Gu, L. Zn Single Atom Catalyst for Highly Efficient Oxygen Reduction Reaction. *Adv. Funct. Mater.* **2017**, *27* (28), 1–6.

(31) Vanhoutte, G.; Hojniak, S. D.; Bardé, F.; Binnemans, K.; Fransaera, J. Fluorine-Functionalized Ionic Liquids with High Oxygen Solubility. *RSC Adv.* **2018**, *8* (9), 4525–4530.

(32) Cheng, Q.; Yang, L.; Zou, L.; Zou, Z.; Chen, C.; Hu, Z.; Yang, H. Single Cobalt Atom and N Codoped Carbon Nanofibers as Highly Durable Electrocatalyst for Oxygen Reduction Reaction. *ACS Catal.* **2017**, *7* (10), 6864–6871.

(33) Long, H.; Pivovar, B. Hydroxide Degradation Pathways for Imidazolium Cations: A DFT Study. *J. Phys. Chem. C* **2014**, *118* (19), 9880–9888.

(34) Islam, M. M.; Imase, T.; Okajima, T.; Takahashi, M.; Niikura, Y.; Kawashima, N.; Nakamura, Y.; Ohsaka, T. Stability of Superoxide Ion in Imidazolium Cation-Based Room-Temperature Ionic Liquids. *J. Phys. Chem. A* **2009**, *113* (5), 912–916.

(35) Rollet, A. L.; Porion, P.; Vaultier, M.; Billard, I.; Deschamps, M.; Bessada, C.; Jouvensal, L. Anomalous Diffusion of Water in [BMIM][TFSI] Room-Temperature Ionic Liquid. *J. Phys. Chem. B* **2007**, *111* (41), 11888–11891.

(36) Wang, Y.; Li, H.; Han, S. A Theoretical Investigation of the Interactions between Water Molecules and Ionic Liquids. *J. Phys. Chem. B* **2006**, *110* (48), 24646–24651.

(37) Köddermann, T.; Wertz, C.; Heintz, A.; Ludwig, R. The Association of Water in Ionic Liquids: A Reliable Measure of Polarity. *Angew. Chemie - Int. Ed.* **2006**, *45* (22), 3697–3702.

(38) Switzer, E. E.; Zeller, R.; Chen, Q.; Sieradzki, K.; Buttry, D. A.; Friesen, C. Oxygen Reduction Reaction in Ionic Liquids: The Addition of Protic Species. *J. Phys. Chem. C* **2013**, *117* (17), 8683–8690.

(39) Hayes, R.; Imberti, S.; Warr, G. G.; Atkin, R. How Water Dissolves in Protic Ionic Liquids. *Angew. Chem., Int. Ed.* **2012**, *51*, 7468–7471.

(40) Chang, T. M.; Dang, L. X.; Devanathan, R.; Dupuis, M. Structure and Dynamics of N, N-Diethyl-N-Methylammonium Triflate Ionic Liquid, Neat and with Water, from Molecular Dynamics Simulations. *J. Phys. Chem. A* **2010**, *114* (48), 12764–12774.

(41) Yoshizawa, M.; Xu, W.; Angell, C. A. Ionic Liquids by Proton Transfer: Vapor Pressure, Conductivity, and the Relevance of ΔpK a from Aqueous Solutions. *J. Am. Chem. Soc.* **2003**, *125* (50), 15411–15419.